Screens Displaying Structural Properties of Aminoacids in Polypeptide Chains: Alanine as a Case Study

Concetta Caglioti[1], Robenilson Ferreira Dos Santos[2,3], Andrea Lombardi[1], Federico Palazzetti[1(✉)], and Vincenzo Aquilanti[1,4]

[1] Dipartimento di Chimica, Biologia e Biotecnologie, Università di Perugia, via Elce di Sotto 8, 06123 Perugia, Italy
federico.palazzetti@unipg.it
[2] Instituto de Fìsica, Universidade Federal da Bahia, Campus Universitario de Ondina, Salvador, BA 40210-340, Brazil
[3] Instituto Federal de Alagoas-Campus Piranhas, Piranhas, AL 57460-000, Brazil
[4] Istituto di Struttura della Materia-Consiglio Nazionale delle Ricerche, 00016 Rome, Italy

Abstract. Large sets of data need to be compacted for classification and extraction of information regarding structural changes of aminoacid units in specific sequences of proteins. The screen is constructed by opposite sides of the virtual tetrahedron built by the six distances between four centers and provides coordinates for a two-dimensional square plot. As alternative *e.g.* to Ramachandran diagrams based on angles, it may offer greater accuracy and sensitivity. The screen was initially employed to peroxides and persulfides, to monitor the distances relevant to chirality changing processes and successively to show some electric and kinetic properties. The smallest chiral aminoacid, alanine, was therefore chosen for the basic illustration presented here. A virtual tetrahedron is built by the six distances between four centers of the aminoacid skeleton: they do not necessarily coincide with bonds, so a computer program permits their calculation from tabulations of experimental and theoretical data. Here, the screen is applied to treat significant geometrical features of alanine as affected by adjacent aminoacids in peptide chains, as available on protein databases. In this exemplary presentation applications of screen plots are limited to biochemistry: elsewhere have been shown useful in other areas, such as spin networks and the kinematics of a four-bar mechanism.

Keywords: Four-center processes · Aminoacid · Quantum angular momentum theory · Protein · Database

© Springer Nature Switzerland AG 2019
S. Misra et al. (Eds.): ICCSA 2019, LNCS 11624, pp. 439–449, 2019.
https://doi.org/10.1007/978-3-030-24311-1_32

1 Introduction

The peptide bond is at the basis of biological chemistry: it constitutes the link between two aminoacids, the building blocks of proteins. It is directly connected to sequences of aminoacids in the protein chain, which forms the primary structure. Experimental information on structure of proteins now includes myriads of compounds inspired by their involvement in areas that span from pharmaceutical and medical chemistry, to biochemistry and biophysics, until astrochemistry and astrobiology [1, 2]. More recent is the explosion of considerable interest by the numerous communities of theoretical and computational chemists (see for example [3]).

This wealth of data is not always homogeneous: accuracies vary and need assessment; also, it may be necessary to fill gaps among data accumulated sparsely on vast but poorly interconnected areas.

To focus on a prototypical study, our choice is to present here the example of the simplest chiral aminoacid, alanine. One of the most debated topics concerns the origin of the homochirality in nature: all aminoacids in proteins are levorotatory, on the contrary sugars involved in biological processes are rigorously dextrorotatory. Many hypotheses have been proposed in the course of the years without reaching unanimous consensus: statistical fluctuations and following amplification that determine the prevalence of one enantiomer; lower energy of one of the two enantiomers due to weak nuclear forces; a possible role played by stereoselectivity in molecular encounters [4–17].

In this paper, we sketch basic theoretical and computational tools for building a representation frame, the "screen", that permits to classify and compact the enormous variety of data on proteins essentially based on information on interatomic distances (this is to be contrasted for example to the Ramachandran plots [18], that report the permitted steric conformations of aminoacids by plotting a pair of dihedral angles typical of the aminoacid unit). The method can be extended to visualize other physico-chemical properties.

The screen representation relies on six distances between four position of atoms in the aminoacids and the diagram is obtained by plotting a pair of "diagonals", according to the classification given for the (not necessarily planar) quadrilaterals that can be individuated in three ways out of any tetrahedron. The screen representation was applied for the first time to a chemical problem specifically for peroxides [19–21] and persulfides [22] to monitor the distances related to chirality changing properties [23] and successively to visualize physico-chemical properties [24]. Here, we report case studies on alanine geometrical features as affected by the aminoacids directly connected, to it in about fifty proteins, whose structural parameters were extracted from Protein Data Bank [25].

The screen representation is not only specifically useful for molecular structure and dynamics: it was initially introduced in quantum angular momentum theory to classify the range of permitted geometries of the tetrahedra related to the vector recoupling and to study spin networks in the semiclassical limit [26]. Lately, it was employed to provide connections between the classical four-bar linkage problem and the theory of $6j$ symbols of quantum mechanical angular momentum theory [27].

The paper is structured as follows: in Sect. 2, we review some fundamental properties of tetrahedra (and lower dimensional projections such as quadrilaterals and quadrangles). The formalism and the basic equations have been adapted from the

theory developed for studies of the Wigner-Racah 6*j* symbols; in Sect. 3, we survey applications to the cases of peroxides and persulfides and introduce the variants needed to the specific case of aminoacids; in Sect. 4, final remarks conclude the paper.

2 The Square Screen Representation of the Six Four-Center Distances

2.1 Elementary Properties of Quadrilaterals, Quadrangles and Tetrahedra

The construction of the screen relies on the geometrical properties of figures with four vertices (quadrilaterals, quadrangles and tetrahedra). A quadrilateral is defined, according to the planar Euclidean geometry, as a polygon with four sides and four angles. The sum of the four inner angles is 360°, a property no longer valid if we admit a three dimensional structure. The lines joining the opposite vertices of quadrilaterals are called diagonals. Their classification relies on the position of the diagonals inside or outside the quadrilateral: a quadrilateral formed by two inner diagonals is convex; it is concave if an inner and an outer diagonal are present; it is called biconcave, if both diagonals are external (the butterfly). In projective and affine geometries, diagonals are considered as further sides, and a complete quadrilateral is formed by four points and six lines.

A complete quadrangle, under most aspects is the same thing but formally is characterized by having four lines incident in six points. In projective geometry, duality permits exchange of role of points and lines, thus the two complete figures are identical, while from an affine viewpoint they are considered different. Extension to three dimension is the usual way that permits to define a tetrahedron, composed by four vertices and six edges on four triangular faces. Considering a tetrahedron of zero volume, or a similar figure obtained by projection on a plane is a way to obtain complete quadrangles, formed by four points and the six joining segments as mentioned above.

There are three ways of choosing couples of diagonals from the six sides of the complete quadrangles and it is possible to define three four-sided figures. The edges a, b, c, d are labelled as follows (according to the "canonical ordering" defined in [26]): a is identified as the shortest side and c is opposite to a, the d side is the longest between the two remaining ones. The two diagonals, x and y, are assigned as follows: x is the one joining the meeting point of a and b with that of c and d, and y is the other one. In conclusion, in a complete quadrilateral one can single out four "sides" (the parameters a, b, c, d) and two "diagonals" (the variables x and y) that represent the abscissa and ordinate of the screen. We also define the minimum values of x and y, respectively x_{min} and y_{min}, and their maximum values, x_{max} e y_{max}, keeping fixed the length of the sides. Their variation range is given by the following relations:

$$\begin{aligned} x_{min} &= b - a \\ x_{max} &= b + a \\ y_{min} &= d - a \\ y_{max} &= d + a \end{aligned} \tag{1}$$

These properties are *e.g.* detailed in [26], see also next section, and show that the screen is confined into a square with sides $x_{max} - x_{min}$ and $y_{max} - y_{min}$, or in the (0–1) range if the sides are properly scaled. In this latter case, the lengths related to the shorter and the longer diagonal must be shortened by $b - a$ or $d - a$ and normalized by $b + a$ or $d + a$, respectively.

2.2 The *Screen* Applied to 6*j*-Symbols

The screen representation was originally developed for and applied to 6*j* symbols, whose entries are designated j_1, j_2, j_3, j_4, j_{12}, j_{23}, to represent the allowed range of existence of the tetrahedron [28, 29] obtained by alternative vector couplings of the four "spins" j_1, j_2, j_3, j_4 through plots of the discrete variables, j_{12} and j_{23} that are intermediate coupling spins (see [29–33]). The six-distance system discussed in Sect. 2.1, in the original representations of the 6*j* symbols of Wigner-Racah coefficients, was introduced to visualize matrix elements between different coupling schemes of quantum mechanical angular momenta (for the applications to 6*j* symbols, see for example [26, 34]). A geometrical interpretation of these elements was given by Wigner and Racah, who associated the lengths of the edges of a generally irregular tetrahedron to the six entries of the 6*j* symbols. Ponzano and Regge [35] investigated the functional dependence of the 6*j* symbol on their entries, arguing that geometrical properties of the tetrahedron, such as volume and dihedral angles, played a role in the amplitude and phase of a semiclassical approximated wave-function. Rigorous derivations, based on earlier work by Neville [36] and Schulten and Gordon [37, 38], and the definitions and the introduction of efficient computational procedures, were developed in [32–34, 39, 40].

2.3 Features of the Screen

Inspired by to the application to the 6*j* symbols, a model of six distances is proposed and employed to plot the tetrahedron associated to a class of molecules, in a 2-dimensional *x*-*y* plane (*x* and *y* are continuous variables in this case): the square "screen" has allowed ranges x_{min}, x_{max}, and y_{min}, y_{max} given in Eq. (1). Here we define some features of the screen. Let *V* be the volume of the tetrahedron (formulas resumed in [32–34]). The caustic line is the curve corresponding to $V = 0$ (a tetrahedron of zero-volume), while the area within the caustic is related to that of a finite volume tetrahedron. The caustic touches the sides of the screen in four points called North, South, East and West gates (N, S, E, W). N is the value of *x* corresponding to the maximum of *y*; on the opposite side, S is the value of *x* for which *y* is the minimum; E is the value of *y* corresponding to the maximum of *x*; finally, W is the value of *y* for which *x* is the minimum. The shape of the caustic, approximately an ovaloid, and the locations of the gates, are typical of the geometry of each examined system assimilated to a tetrahedron.

Ridges are curves that mark configurations of the associated tetrahedron when two specific pairs of triangular faces are orthogonal [26]. Formulas to calculate the location of the gates, the equations of the caustic and the ridges, and the volume of the associated tetrahedron are given in [27] and references therein.

2.4 Screen Representations of Peroxides and Persulfides

Screen representations of peroxides and persulfides have been discussed in Refs. [23]. Molecules of this class are schematically represented by the formula R1 – O1 – O2 – R2 for peroxides, and R1 – S1 – S2 – R2 for persulfides, where O1 – O2 are the oxygens forming the peroxidic bond (or S1 – S2 the sulfurs of the persulfidic bond), and R1 and R2 are the atoms or groups connected to O1 and O2 (or S1 and S2), respectively.

One can individuate three distances corresponding to the bond lengths between the atom (or group) R1 and the O1 atom, between the atoms O1 and O2, and between the atom O2 and the atom (or group) R2, these distances lie along the three bonds that identify the stereogenic units of peroxides (see Fig. 1 of Ref. [23]). Three additional distances are given by R1 – O2, R2 – O1, and R1 – R2. This 6-distance system defines a tetrahedron that, when confined or projected in the plane results in a "quadrangle", whose joints are precisely the elements of the stereogenic unit. As mentioned previously, in principle all three pairs of distances can be plotted, however in this case R1 – R2 is the most suitable one to monitor the chirality changing processes. Thus, R1 – O1, R1 – O2, R2 – O1, R2 – O2 are selected as the sides of the "quadrilateral", while the distances O1 – O2 and R1 – R2 are diagonals of the quadrilateral, *i.e.* the variables. It must be noted, see Ref. [23], that ridges connect the geometries of persulfides or peroxides, (*cis*, equilibrium and *trans*).

3 Screen Representation of Peptides

Screens are now shown to display structural properties of proteins taken from Protein Data Bank [25]. Here, we list those proteins included in the screen, all involving alanine. For each protein chosen given in order of complexity from small to longer ones, we report the four-character code, the name of the peptide, the organism from which it was isolated, and in parenthesis the number of the aminoacid residues:

5aht Isomerase *H. Sapiens* (43), 5jpx Metal binding protein *H. Sapiens* (45), 1hgv Coat protein filamentous bacteriophage (46), 1hgz Coat protein filamentous bacteriophage (46), 1hh0 Coat protein filamentous bacteriophage (46), 1nh4 Coat protein filamentous bacteriophage (50), 2n8t Ligase *R. norvegicus* (53), 1new Cytochrome (electron transport) *D. acetoxidans* (68), 5lg7 Ligase *H. Sapiens* (69), 2ltf Viral protein (Tail protein) *Escherichia phage P2* (71), 2cqj RNA binding protein *H. Sapiens* (71), 6axd Transferase *H. Sapiens* (72), 2lze Ligase *E. coli* (87), 1x4q RNA binding protein *H. Sapiens* (92), 1e1g Human prion protein (104), 1e1j Human prion protein (104), 1e1p Human prion protein (104), 1e1s Human prion protein (104), 1e1u Human prion protein (104), 1e1w Human prion protein (104), 1hjm Human prion protein (104), 1hjn Human prion protein (104), 2l9q Heat shock protein *S. cerevisiae* (109), 1xyk Canine prion protein (111), 1xyj Cat prion protein (111), 1xyw Elk prion protein (111), 2ku4 Horse prion protein (113), 6gt7 Transferase *S. islandicus* (115), 1lwb Hydrolase *S. violaceoruber* (122), 1k8h RNA binding protein *A. aeolicus* (133), 5v7z Signaling protein *H. Sapiens* (132), 6do6 Lipid binding protein *H. Sapiens* (135), 2fe0 Protein transport (membrane protein) *L. major* (136), 6do7 Lipid binding protein *H. Sapiens* (142), 5w4s Transferase *R. norvegicus* (151), 2lu5 Oxidoreductase *H. Sapiens* (153),

2i83 Cell adhesion *H. Sapiens* (160), 1qlx Human prion protein (210), 1qlz Human prion protein (210), 6f2x Transferase *M. tuberculosis* (216), 5lg0 Ligase *H. Sapiens* (223), 2h35 Oxygen storage/transport *H. Sapiens* (574), 2m6z Oxygen transport *H. Sapiens* (574), 5kk3 Protein fibril *H. Sapiens* (756), 4gdi Neuraminidase Influenza A virus (2238).

Here, we discuss structural features plotting significant distances related to the peptidic bond, no attention being payed to caustics and ridges. See [23] of relevance for dynamics (*e.g.* changes of chirality) to be considered in future work.

In Fig. 1, we report an example of the virtual tetrahedron built in an aminoacid unit, specifically alanine. The four vertices are the atoms directly bounded to the asymmetric carbon atom denoted by C_A, the nitrogen atom N, one of the hydrogen atoms H_A, the carboxylic carbon C and the carbon of the alanine C_B. The six distances that form the edges of the virtual tetrahedron are N-H_A, N-C_B, N-C, H_A-C_B, H_A-C, C-C_B. The screen is a plot having as coordinate a couple of two opposite distances, that can be chosen in three ways: N-H_A and C-C_B, N-C_B and H_A-C; N-C and H_A-C_B. The caustic curve, described in the previous section but not presented here, would delimit the field of existence of the tetrahedron of zero volume, that corresponds to a planar quadrangle, *i.e.* with the four vertices that lie on the same plane. Being the arrangement of the four atoms in general vertices of a tetrahedron of non zero volume, the points are placed internally to the caustic.

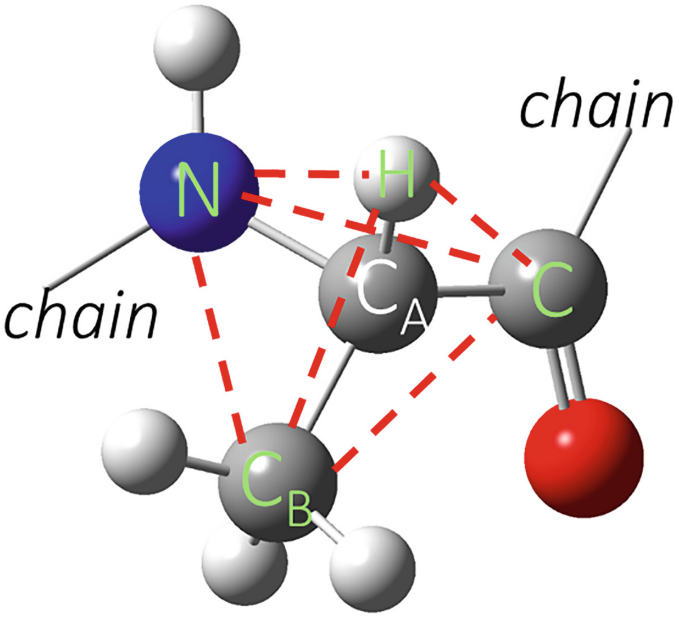

Fig. 1. In the virtual tetrahedron built in the aminoacid unit (alanine), dashed red lines are the six edges joining the four vertices that are: the nitrogen denoted by N (in blue), the carbon atom of the lateral chain CH_3 denoted by C_B (in grey), the hydrogen connected to the central α-carbon H_A (in white), the carboxylic carbon atom C (in grey). Note that the central α-carbon, C_A (in grey) is not a vertex: it is located at the center of the tetrahedron and in grey we indicate the four chemical bonds. (Color figure online)

In Fig. 2, we report the screen of the distances $H_A - C_B$ and N – C of alanine. The red dot at $H_A - C_B$ 2.16 Å and N – C 2.47 Å corresponds to the geometry of the most stable conformer of isolated alanine [41]. Adding substituents in the N side of the unit or in the C side unit, the $H_A - C_B$ length (y) may shrink from *ca.* 2.15 to *ca.* 2.0, while the N – C length (x) varies from 2.45 Å to the range 2.3 – 2.6 Å. The points can be classified into two main regions: the first one with the H_A – CB distance lower than 2.1 Å and concentrated in the range of distances N – C between 2.35 Å and 2.5 Å. The second one is located at values of the $H_A - C_B$ distance higher than 2.1 Å and span a wider range of N – C distances, between 2.25 Å and 2.6 Å. Future work should distinguish shortening and lengthening according to the nature of connected aminoacids.

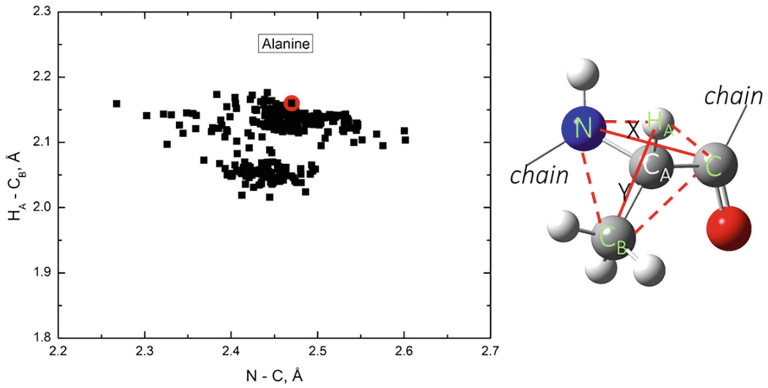

Fig. 2. Screen of the distances (in angstrom) $H_A - C_B$ *vs.* N – C in alanine. The red dot shows the distances corresponding to the most stable conformer of isolated alanine. On the right, the tetrahedron built on the aminoacid, continuous red lines showing the diagonals X (N – C distance) and Y ($H_A - C_B$ distance). (Color figure online)

In Fig. 3, we report the screen of the distances $N - H_A$ and $C - C_B$ of alanine. The red dot at $N - H_A$ 2.15 Å and $C - C_B$ 2.51 Å corresponds to the geometry of the most stable conformer of isolated alanine [41]. Adding substituents in the N side of the unit or in the C side unit, the $N - H_A$ length (y) may shrink from *ca.* 2.1 to *ca.* 1.95 Å, while the $C - C_B$ length (x) varies from 2.5 Å to 2.35 – 2.6 Å.

In Fig. 4, we report the screen of the distances $N - C_B$ and H_A – C of alanine. The red dot at H_A – C 2.13 Å and $N - C_B$ 2.48 Å [41] corresponds to the geometry of the most stable conformer of isolated alanine [41]. Adding substituents in the N side of the unit or in the C side unit, the $N - C_B$ length (y) may vary from 2.48 Å to *ca.* 2.35 – 2.55 Å, while the H_A – C length (x) varies from 2.13 Å to *ca.* 2.05 – 2.2 Å. The points are distributed between two main regions: the first one at values of the H_A – C distance lower than 2.1 Å and the second one with values of the H_A – C distance included between 2.1 and 2.2 Å.

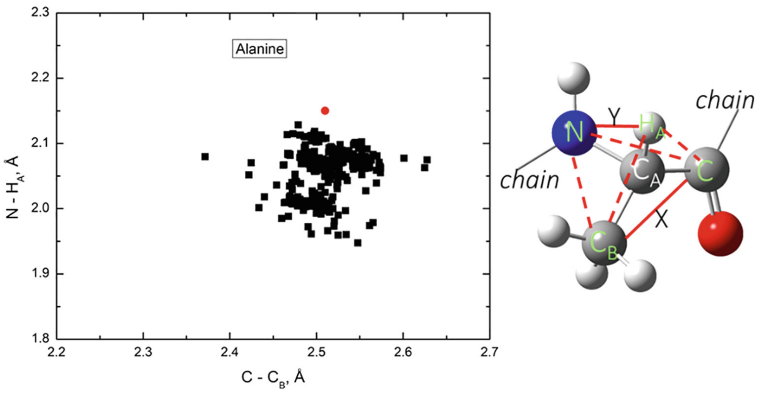

Fig. 3. Screen of the distances (in angstrom) N – H_A *vs.* C – C_B in alanine. The red dot shows the distances corresponding to the most stable conformer of isolated alanine. On the right, the tetrahedron built on the aminoacid, continuous red lines show the diagonals *X* (C – C_B distance) and *Y* (N – H_A distance). (Color figure online)

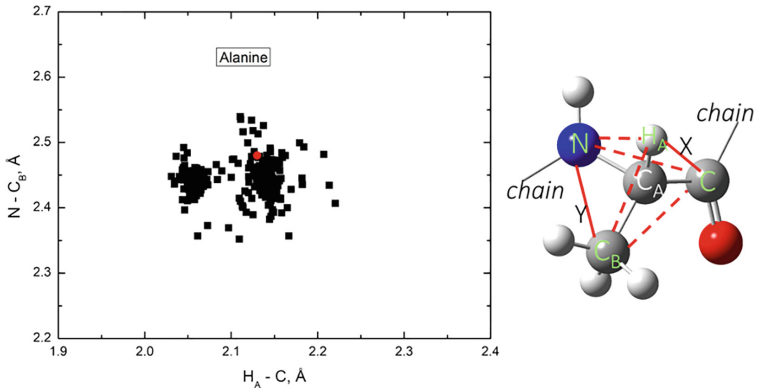

Fig. 4. Screen of the distances (in angstrom) N – C_B *vs.* H_A – C in alanine. The red dot shows the distances corresponding to the most stable conformer of isolated alanine. On the right, the tetrahedron built on the aminoacid, continuous red lines showing the diagonals *X* (H_A – C distance) and *Y* (N – C_B distance). (Color figure online)

4 Final Remarks

The square screen serves to display molecular properties by properly plotting significant distances among not necessarily bonded atoms. Here, it has been applied to the structural properties related to alanine in peptides.

It is important to point out that among the choices of distances that can be in principle done, most representative are those between atoms present in all the aminoacids, *i.e.* those atoms directly connected to the central α-carbon. The variation of distances are expected to be related to the structure of the protein under the action of the peptide chain environment.

The choice of distances in our plot is arguably showing a better alternative perspective with respect to that of dihedral angles, because they can be extracted directly from the most common and employed databases. Also shortening or lengthening of bonds can be intuitively correlated to increasing or decreasing binding energies. It has been shown that this approach is suitable to treat systems not exclusively related to these classes of molecules, and in general the algorithms will allow to deal with extensive inputs from databases much wider than considered here.

In future applications, moving from structure to dynamics, the caustics and ridges can be profitably calculated and exhibited on screens, both to represent the field of existence of the intra- and inter-aminoacid unit distances, and to monitor the dynamical processes related for example to change of chirality.

Acknowledgements. The authors acknowledge the Italian Ministry for Education, University and Research, MIUR, for financial supporting through SIR 2014 Scientific Independence for young Researchers (RBSI14U3VF).

Bibliography

1. Palazzetti, F., Maciel, G.S., Lombardi, A., Grossi, G., Aquilanti, V.: The astrochemical observatory: molecules in the laboratory and in the cosmos. J. Chin. Chem. Soc. **59** (2012). https://doi.org/10.1002/jccs.201200242
2. Gianturco, F.A., et al.: Exploring a chemical route for the formation of stable anions of polyynes [Cn H−(n = 2, 4)] in molecular clouds. Astrophys. J. **830**, 2 (2016). https://doi.org/10.3847/0004-637X/830/1/2
3. Wang, X., Li, Y., Yang, Z., Lu, C., Zhu, T.: A quantum mechanical computational method for modeling electrostatic and solvation effects of protein. Sci. Rep. **8**, 5475 (2018)
4. Lombardi, A., Palazzetti, F., Aquilanti, V., Pirani, F., Casavecchia, P.: The astrochemical observatory: experimental and computational focus on the chiral molecule propylene oxide as a case study. In: Gervasi, O., et al. (eds.) ICCSA 2017. LNCS, vol. 10408, pp. 267–280. Springer, Cham (2017). https://doi.org/10.1007/978-3-319-62404-4_20
5. Palazzetti, F., et al.: Stereodirectional photodynamics: experimental and theoretical perspectives. In: AIP Conference Proceedings, vol. 1790, p. 020020 (2016). https://doi.org/10.1063/1.4968646
6. Kasai, T., et al.: Directions of chemical change: experimental characterization of the stereodynamics of photodissociation and reactive processes. Phys. Chem. Chem. Phys. **16**, 9776–9790 (2014). https://doi.org/10.1039/c4cp00464g
7. Barreto, P.R.P., et al.: Potential energy surface for the interaction of helium with the chiral molecule propylene oxide. In: Gervasi, O., et al. (eds.) ICCSA 2018. LNCS, vol. 10964, pp. 593–604. Springer, Cham (2018). https://doi.org/10.1007/978-3-319-95174-4_46
8. Su, T.-M., Palazzetti, F., Lombardi, A., Grossi, G., Aquilanti, V.: Molecular alignment and chirality in gaseous streams and vortices. Rend. Lincei **24**, 291–297 (2013). https://doi.org/10.1007/s12210-013-0249-x
9. Che, D.-C., Kanda, K., Palazzetti, F., Aquilanti, V., Kasai, T.: Electrostatic hexapole state-selection of the asymmetric-top molecule propylene oxide: rotational and orientational distributions. Chem. Phys. **399**, 180–192 (2012). https://doi.org/10.1016/j.chemphys.2011.11.020

10. Lombardi, A., Maciel, G.S., Palazzetti, F., Grossi, G., Aquilanti, V.: Alignment and chirality in gaseous flows. J. Vac. Soc. Jpn. **53**, 645–653 (2010). https://doi.org/10.3131/jvsj2.53.645
11. Albernaz, A.F., Barreto, P.R.P., Aquilanti, V., Lombardi, A., Palazzetti, F., Pirani, F.: The astrochemical observatory: the interaction between helium and the chiral molecule propylene oxide. In: AIP Conference Proceedings, vol. 2040, p. 020018 (2018). https://doi.org/10.1063/1.5079060
12. Lin, K.-C., et al.: Angular distribution of bromine atomic photofragment in oriented 2-bromobutane via hexapole state selector. In: AIP Conference Proceedings, p. 020001 (2017). https://doi.org/10.1063/1.5012287
13. Nakamura, M., et al.: Stereodirectional images of molecules oriented by a variable-voltage hexapolar field: fragmentation channels of 2-bromobutane electronically excited at two photolysis wavelengths. J. Chem. Phys. **147** (2017). https://doi.org/10.1063/1.4981025
14. Falcinelli, S., et al.: Double photoionization of propylene oxide: a coincidence study of the ejection of a pair of valence-shell electrons. J. Chem. Phys. **148**, 114302 (2018). https://doi.org/10.1063/1.5024408
15. Lombardi, A., Palazzetti, F., Aquilanti, V., Grossi, G.: Chirality in molecular collisions. In: AIP Conference Proceedings, vol. 1906, p. 030012 (2017). https://doi.org/10.1063/1.5012291
16. Aquilanti, V., et al.: The astrochemical observatory: computational and theoretical focus on molecular chirality changing torsions around O–O and S–S bonds. In: AIP Conference Proceedings, vol. 1906, p. 030010 (2017). https://doi.org/10.1063/1.5012289
17. Che, D.-C., Palazzetti, F., Okuno, Y., Aquilanti, V., Kasai, T.: Electrostatic hexapole state-selection of the asymmetric-top molecule propylene oxide. J. Phys. Chem. A **114**, 3280–3286 (2010). https://doi.org/10.1021/jp909553t
18. Carrascoza, F., Zaric, S., Silaghi-Dumitrescu, R.: Computational study of protein secondary structure elements: Ramachandran plots revisited. J. Mol. Graph. Model. **50**, 125–133 (2014)
19. Lombardi, A., Palazzetti, F., Maciel, G.S., Aquilanti, V., Sevryuk, M.B.: Simulation of oriented collision dynamics of simple chiral molecules. Int. J. Quantum Chem. **111**, 1651–1658 (2011). https://doi.org/10.1002/qua.22816
20. Barreto, P.R.P., Palazzetti, F., Grossi, G., Lombardi, A., Maciel, G.S., Vilela, A.F.A.: Range and strength of intermolecular forces for van der Waals complexes of the type H2Xn-Rg, with X = O, S and n = 1, 2. Int. J. Quantum Chem. **110**, 777–786 (2010). https://doi.org/10.1002/qua.22127
21. Barreto, P.R.P., Vilela, A.F.A., Lombardi, A., Maciel, G.S., Palazzetti, F., Aquilanti, V.: The hydrogen peroxide-rare gas systems: quantum chemical calculations and hyperspherical harmonic representation of the potential energy surface for atom-floppy molecule interactions. J. Phys. Chem. A **111**, 12754–12762 (2007). https://doi.org/10.1021/jp076268v
22. Maciel, G.S., Barreto, P.R.P., Palazzetti, F., Lombardi, A., Aquilanti, V.: A quantum chemical study of H2S2: intramolecular torsional mode and intermolecular interactions with rare gases. J. Chem. Phys. **129**, 164302 (2008). https://doi.org/10.1063/1.2994732
23. Aquilanti, V., Caglioti, C., Lombardi, A., Maciel, G.S., Palazzetti, F.: Screens for displaying chirality changing mechanisms of a series of peroxides and persulfides from conformational structures computed by quantum chemistry. In: Gervasi, O., et al. (eds.) ICCSA 2017. LNCS, vol. 10408, pp. 354–368. Springer, Cham (2017). https://doi.org/10.1007/978-3-319-62404-4_26

24. Caglioti, C., Santos, R.F.D., Aquilanti, V., Lombardi, A., Palazzetti, F.: Screen mapping of structural and electric properties, chirality changing rates and racemization times of chiral peroxides and persulfides. In: AIP Conference Proceedings, vol. 2040, p. 020021 (2018). https://doi.org/10.1063/1.5079063
25. Protein Data Bank, PDB. https://www.rcsb.org/
26. Bitencourt, A.C.P., Ragni, M., Littlejohn, R.G., Anderson, R., Aquilanti, V.: The screen representation of vector coupling coefficients or Wigner 3*j* symbols: exact computation and illustration of the asymptotic behavior. In: Murgante, B., et al. (eds.) ICCSA 2014. LNCS, vol. 8579, pp. 468–481. Springer, Cham (2014). https://doi.org/10.1007/978-3-319-09144-0_32
27. Aquilanti, V., et al.: Quadrilaterals on the square screen of their diagonals: Regge symmetries of quantum mechanical spin networks and Grashof classical mechanisms of four-bar linkages. Rend. Lincei **30**, 67–81 (2019). https://doi.org/10.1007/s12210-019-00776-x
28. Littlejohn, R.G., Yu, L.: Uniform semiclassical approximation for the Wigner 6j-symbol in terms of rotation matrices. J. Phys. Chem. A **113**, 14904–14922 (2009)
29. Aquilanti, V., Haggard, H.M., Hedeman, A., Jeevangee, N., Littlejohn, R., Yu, L.: Semiclassical mechanics of the Wigner 6j-symbol. J. Phys. A. **45**, 065209 (2012)
30. Aquilanti, V., Capecchi, G.: Harmonic analysis and discrete polynomials from semiclassical angular momentum theory to the hyperquantization algorithm. Theoret. Chem. Acc. **104**, 183–188 (2000)
31. De Fazio, D., Cavalli, S., Aquilanti, V.: Orthogonal polynomials of a discrete variable as expansion basis sets in quantum mechanics the hyperquantization algorithm. Int. J. Quantum Chem. **93**, 91–111 (2003)
32. Aquilanti, V., Cavalli, S., De Fazio, D.: Angular and hyperangular momentum coupling coefficients as hahn polynomials. J. Phys. Chem. **99**, 15694–15698 (1995)
33. Bitencourt, A.C.P., Marzuoli, A., Ragni, M., Anderson, R.W., Aquilanti, V.: Exact and asymptotic computations of elementary spin networks: classification of the quantum–classical boundaries. In: Murgante, B., et al. (eds.) ICCSA 2012. LNCS, vol. 7333, pp. 723–737. Springer, Heidelberg (2012). https://doi.org/10.1007/978-3-642-31125-3_54
34. Aquilanti, V., Bitencourt, A.C.P., da S. Ferreira, C., Marzuoli, A., Ragni, M.: Combinatorics of angular momentum recoupling theory: spin networks, their asymptotics and applications. Theoret. Chem. Acc. **123**, 237 (2009)
35. Ponzano, G., Regge, T.: Semiclassical limit of Racah coefficients. In: Spectroscopic and Group Theoretical Methods in Physics. North-Holland, Amsterdam (1968)
36. Neville, D.: A technique for solving recurrence relations approximately and its application to the 3j and 6j symbols. J. Math. Phys. **12**, 2438 (1971)
37. Schulten, K., Gordon, R.: Semiclassical approximations to 3j- and 6j-coefficients for quantum-mechanical coupling of angular momenta. J. Math. Phys. **16**, 1971–1988 (1975)
38. Schulten, K., Gordon, R.: Exact recursive evaluation of 3j- and 6j-coefficients for quantum mechanical coupling of angular momenta. J. Math. Phys. **16**, 1961–1970 (1975)
39. Ragni, M., Bitencourt, A.C.P., Aquilanti, V., Anderson, R.W., Littlejohn, R.G.: Exact computation and asymptotic approximations of 6j symbols: illustration of their semiclassical limits. Int. J. Quantum Chem. **110**, 731–742 (2010)
40. Aquilanti, V., Cavalli, S., Coletti, C.: Angular and hyperangular momentum recoupling, harmonic superposition and Racah polynomials: a recursive algorithm. Chem. Phys. Lett. **344**, 587–600 (2001)
41. Berlin ab-initio amino acid DB. http://aminoaciddb.rz-berlin.mpg.de/